Pressure measurements of the detachment bubble on the Bolund Island

Tee Seong Yeow[a], *Alvaro Cuerva-Tejero*[b], *Javier Pérez Alvarez*[c]

[abc] Instituto Ignacio Da Riva, Universidad Politécnica de Madrid, 28040 Madrid, Spain.
Corresponding author: teeseong.yeow@upm.es Tel: 0034 91 336 63 53/54

Pressure measurements on the surface of a 1:230 scale model of Bolund Island are presented. The model is smooth and no roughness elements for boundary layer generation have been considered since the experiment is designed as the simplest possible reference case. Measurement have been taken for a range of Reynolds numbers based on the average undisturbed wind speed U_∞ and the maximum height of the island, h [1.7×10^4, 8.5×10^4], and for a range of wind directions. Three minutes time series of pressure in more than 400 points have been acquired and analysed to obtain the spatial distribution of both the time average and the variance of the pressure coefficient signal. The horizontal extension of the detachment bubble for the different Reynolds numbers and wind directions is identified by isobars and curves of constant value of pressure variance. The applicability of this technique for evaluating the horizontal topology of high turbulence regions associated to detachment bubbles after escarpments in potential wind farm sites is analysed. The results obtained show that the behaviour of the mean pressure coefficient, C_p, the std. pressure coefficient, $C_{\sigma p}$, and the skewness of the pressure, S_p can be used to study the bubble over the island to a certain extent.

1 INTRODUCTION

Recently, two new test cases have been proposed for benchmarking of numerical and physical modelling of complex terrain flows, these are the Alaiz test case [see Conan et al., 2011] and the Bolund experiment [see Bechmann et al., 2009]. The Bolund experiment was initiated by Risϕ DTU as a blind comparison of different numerical models (including linear, RANS and LES simplifications of Navier-Stokes equations). More detailed description of the blind comparison can be found in Bechmann et al [2009]. The main conclusions from the initial analysis are: *a*) a large scatter of the numerical results exists (mainly in the vicinity of the island escarpment, *b*) the mean velocities are better predicted than turbulent kinetic energy (TKE), and *c*) the best models predicting both, mean wind speed and TKE are the RANS models with two closure equations.

One of the main geometric characteristics of the Bolund island is the escarpment facing approximately the wind directions 200º to 295º (see figure 3). It can be idealised as a combination of a 50º ramp extending from the sea level to 0.5h, plus an almost vertical step from 0.5h to h, being h the total height of the escarpment. The escarpment height varies slightly in the interval 200º-295º being roughly the maximum height of the island (11.73 m). This geometry guarantees that flow detaches at the edge (with a sufficiently large Reynolds number) while the flat top ensures reattachment of the flow on the island. This flow pattern on Bolund island has been preliminary documented by smoke visualizations in wind tunnel in Bechmann et al. [2009] and quantified by direct measurement of very high values of TKE on the real field in the met masts close to the escarpment for heights below 2 m (met masts M2 and M6 for 239º and 270º wind directions respectively).

The detached-reattaching flow structures, in Bradshaw's wordings, can provoke a *weak*, *strong* or an *overwhelming* perturbation in the approaching flow [see Bradshaw & Wong, 1972] depending on the relation δ/h (>>1, $O(1)$, <<1, respectively) being δ the size of the incoming shear layer, producing from a slight change to a complete mutation of the original flow structure. The preliminary studies of the incoming boundary layer at Bolund island (for 239º and 270º wind directions) indicate a minimum value for the ratio of the boundary layer thickness, δ, to the escarpment height, $\delta/h \approx 1.5$, and therefore $\delta/h \approx O(1)$.

The most relevant references for understanding the detached-reattaching zone on the Bolund island have been considered the existing studies on blunt flat plates with right-angled corners [BFP, see, for instance, Kiya & Sasaki, 1983a & 1983b or Nakamura & Ozono, 1987] and forward-facing steps with right-angled corners [FFS, see for instance Tachie et al. 2001 or

Largeau & Moriniere, 2007]. The geometry of BFP and FFS are defined by the BFP thickness, a=2h, or the FFS height, h; and for both geometries, their width, d, and length, l. The studies on FFS and BFP have been focused on three main aspects, *a*) the flow topology at the detached-reattaching zone, *b*) the relaxation process of the new boundary layer after reattachment and *c*) the surface pressure topology beneath the bubble region and upstream-downstream it and its relation with the flow field in its vicinity, both inside and outside of the detachment bubble. The study of the surface pressure topology just under and close to the detachment bubble on simple geometries (such as the mentioned FFS and BFP) has been an issue of direct concern in the understanding of wind loads on bluff bodies like buildings [Li & Melbourne, 1995].

Additionally, the study of the pressure field topology on the top surface of BFP and FFS has been established as an adequate diagnostic means for the determination of the size and the intensity on the detached-reattaching zone [Hillier & Cherry, 1981, Castro & Dianat, 1983, Kiya & Sasaki, 1983a & 1983b, Saathoff & Melbourne, 1989, Li & Melbourne, 1995, Li & Melbourne, 1999, Largeau & Moriniere, 2007, Sherry et al., 2010] as well as a methodology to determine the influence of scale parameters such as Re_h, δ/h or the ratio of the longitudinal component in the longitudinal direction to the body height, L_u^x/h or pure inflow parameters such as the turbulence intensity of the longitudinal component of flow velocity, I_u on the bubble characteristics.

Therefore the methodology could be quite appropriate to determine the fidelity of wind tunnel tests. Taking this into account, the authors have considered interesting to analyse the pressure behaviour on the surface of a model of the Bolund Island in order to gain insight in the bubble topology likely formed on the flat part to the island. The paper is organised in three main parts: the first covering background study, a description of the bubble phenomenon and the non-dimensional numbers describing it and the second covering instrumentation and wind tunnel setup followed by results obtained and finally conclusions.

2 MAIN CHARACTERISTICS OF THE DETACHED-REATTACHING BUBBLE

Let us consider as a reference flow configuration for our test a rectangular body of dimensions l×d×h, located on the surface on a channel flow and immersed in a neutrally stratified boundary layer with thickness δ, free mean wind speed, U_∞, square root of the free wind speed variance, $\sigma_{u\infty}$ and the longitudinal integral length scale L_u^x. The dimensional analysis allows to describe the ensemble averaged flow topology by non-dimensional parameters l/h, d/h, Re_h, δ/h, L_u^x/h and finally $I_u = \sigma_{u\infty}/U_\infty$. Of course any ensemble mean parameter will also depends on the non-dimensional coordinates x/h, y/h and z/h but not on time, since the flow field is stationary. The aspect ratios l/h and d/h affect considerably to the flow topology in front of the body and downstream the edge [see Sherry at al., 2010]. l/d must be large enough to assure that the forward-step is truly *isolated* (Sherry's wording) meaning that the flow field at the front is not affected by the downstream wake of the body. Regarding the span-wise aspect ratio d/h, works like Hillier & Cherry [1981] or Kiya & Sasaki [1983a & 1983b] establish values d/h >10 to assure 2D mean conditions at the central part of the body [see Largeau & Moriniere, 2007]. Obviously the Bolund topography is not fulfilling the geometric requirements to be considered as a 2D configuration with a FFS truly *isolated* but the analysis of such an idealised configuration can provide certain insight on the topology of the detachment. In the figure 1 an schematic on the ensemble mean velocity field on a 2D (d/h>>1), truly *isolated* (l/d>>1) FFS is shown.

It is quite well established that when the flow approaches the FFS, the blockage provoked by the vertical wall generates a severe adverse pressure gradient. As a consequence a first detachment bubble (see figure 1) is initiated at a mean position $[x/h, z/h] \approx [(-0.8, -1.5),0]$, so $l_F/h \approx (-0.8, -1.5)$. The flow reattaches to the vertical wall at a mean position $[x/h, z/h] \approx [0,(0.6,0.65)]$, [see Sherry et al., 2010 and Huiyin & Yanhua., 2011]. The dynamics of this first detachment bubble is complex even for a 2D- truly *isolated* FFS in both laminar and turbulent conditions [see results and analysis for $\mathrm{Re}_h \in [940,8400]$ in Stuer et al., 1999 and the analysis in Largeau & Moriniere, 2007]. This first detachment bubble acts a fluid ramp and its width seems to depend on δ/h.

On the top surface of the FFS, just at the edge, a second separation of the flow is produced (therefore at [x/h, z/h] = [0,1]). A shear layer with high TKE evolves from the edge adjusting the velocity from the reverse flow region inside the bubble to the free conditions. The ratio δ/h influences notably the length of the bubble, l_R/h, when δ/h>1, since, depending on the specific value of δ/h, the FFS can interact with the viscous layer, with the log layer or the outer layer of the incident boundary layer [see Tachie et al., 2001 and Sherry et al., 2010].

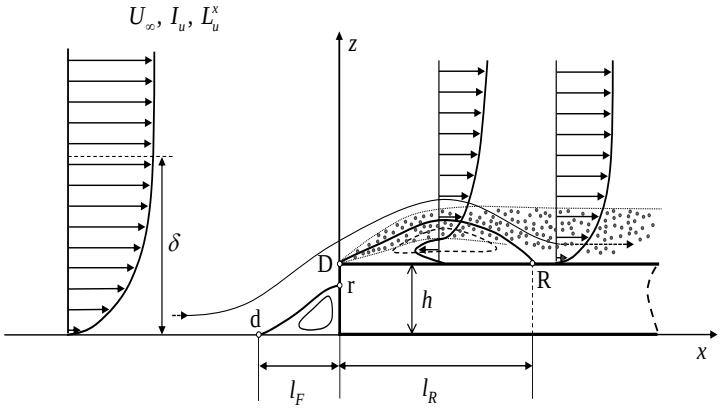

Figure 1: Schemantic of the ensemble mean flow velocity field around a 2D-truly *isolated* FFS [adapted from Sherry et al., 2010 and Bradshaw & Wong, 1972]. d: mean position of the detachment point in front of the FFS, r: mean position of the reattachment point on the vertical wall, D: position of the detachment point on top of the FSS (edge), R: mean position of the reattachment on top of the FFS. l_F is the mean length of the front separation bubble and l_R is the mean length of the separation bubble on top of the FFS. The shear layer originated at D is schematised with grey dots.

The Reynolds number, Re_h, is another important parameter. There is a growing dependence of the non-dimensional length of the bubble, l_R/h, with Re_h, In Sherry et al. [2010] a mechanism of detachment at the FFS edge is proposed as responsible for the high sensitivity of l_R/h with Re_h for Re_h<8500. For very low Re_h, laminar separation occurs at the edge of the FFS followed by laminar to turbulent transition and finally a turbulent reattachment at a certain distance on top of the FFS. The transition distance which can be used to describe the topology of the bubble decreases to zero as Re_h increase till $Re_h \approx 8500$ where the detachment is fully turbulent. For Re_h > 8500 there is not any change in the characteristics of the detachment (this is fully turbulent) so that the sensitivity of l_R/h on Re_h, although still positive, is much smaller in opinion of Sherry et al. However the data from Largeau & Moriniere indicate that the sensitivity is still important. Both data sets where obtained for similar I_u (0.015) but for different value of δ/h, much smaller in the case of Largeau & Moriniere (what is in accordance with a larger value of l_R/h). In the case of Camussi et al., the remarkably lower value of l_R/h could be explained both by a higher value of δ/h and I_u. The ratio L_u^x/h is not indicated in any case, being this a source of uncertainty.

The formation of the bubble on the top of the FFS and BFP can be briefly described by the accumulation of vorticity contributing to the growth of the bubble [see Sherry et al., 2010 and Kiya & Sasaki, 1983b]. After a certain time, a large scale vortex is ejected, and the bubble size decreases, the process of vorticity accumulation repeating again. This dynamic process is responsible of the instantaneous change of the reattachment line (so that l_R/h as a defined line can be only determined as a mean characteristic) and it is known as “flapping” [Camussi et al., 2008]. Finally, several authors [see Kiya & Sasaki, 1983b, Largeau & Moriniere, 2007, Camussi et al., 2008] have identified that the mean convection velocity of vortex structures on the FFS in the bubble ranges from $0.3U_\infty$ close to the front, up to $0.7U_\infty$ well after the reattachment zone, being in the order of 0.5 U_∞ at the reattachment. All these studies [Hillier & Cherry, 1981, Nakamura & Ozono, 1986, Saathoff & Melbourne, 1989, Li & Melbourne, 1995, 1999] agree in a length of the bubble $l_R/(2h) \approx (3.5,5)$ for the reference smooth case. A general agreement exists on the influence of I_u on the longitudinal size of the bubble l_R/h. Larger values of longitudinal turbulence intensity lead to smaller bubbles, so l_R/h decreases as I_u increases. At the same time

the bubble is more intense, for instance, the minimum mean pressure coefficient C_p under the detached zone is smaller (more negative), or the maximum standard deviation pressure coefficient, $C_{\sigma p}$, is larger as I_u grows.

3 STATISTICS DERIVED FROM SURFACE PRESSURE AS DIAGNOSTIC PARAMETERS OF THE BUBBLE EXTENSION

It has been mentioned that largely negative mean pressure coefficients beneath the bubble are associated to the accumulation of vortices originated at the edge in the bubble [Kiya & Sasaki, 1983a & 1983b, Largeau & Moriniere, 2007, Camussi et al., 2008]. So the existence/intensity of the bubble can be preliminary diagnosed from the exploration of the C_p. Additionally, different authors have identified the reattachment region with that part on the FFS where the variation of mean C_p with x/h is largest [Hillier & Cherry, 1981, Li & Melbourne, 1999] being this region roughly coincident with the location where the standard deviation of the pressure coefficient, $C_{\sigma p}$, is maximum. Most of the referred studies have analysed the influence of parameters such as I_u, or L_u^x/h on the functions $C_p(x/h)$ or $C_{\sigma p}(x/h)$ [Nakamura & Ozono, 1986 and Li & Melbourne, 1995, 1999 are representative examples] inferring characteristics of the bubble such as its length l_R/h from the location of max[dC_p/d(x/h)] or max($C_{\sigma p}$).
Kiya & Sasaki [1983*b*] and Saathoff & Melbourne [1989] argue that the entrainment of outer energetic fluid into the bubble at the reattachment zone provokes a larger probability of positive peaks of the pressure fluctuation originating an asymmetry around the mean of the PDF of the pressure fluctuation which is quantified by large positive values of the pressure skewness, S_p. Camussi et al. [2008] also agree with this reasoning. The mentioned authors identified, by means of PIV, a bubble length $l_R/h \approx 2.1$ for $Re_h = 2.63\times10^4$, and calculate the PDF of the pressure fluctuation at x/h = 0.45, 1.95 and 2.7, finding that the PDF is skewed negatively at x/h = 0.45 and positively at x/h = 1.95 and mainly at x/h = 2.7. In Camussi et al. [2008] are also determined largely positive values of S_p upstream of the front of the FFS also in agreement with the findings of Steinwolf & Rizzi [2006]. In figure 6, and schematic of the process for the determination of the bubble length l_R/h based on the behaviour of the mean pressure coefficient, C_p, the std. pressure coefficient, $C_{\sigma p}$, and the skewness of the pressure, S_p is shown.

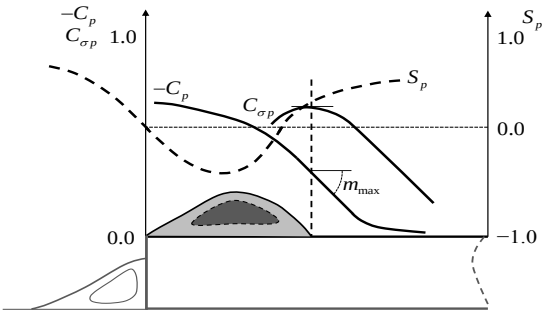

Figure 2: Schematic on the diagnostic process on the bubble length l_R/h based on the behaviour of the mean pressure coefficient, C_p, the std. pressure coefficient, $C_{\sigma p}$, and the skewness of the pressure, S_p.

4 EXPERIMENTAL SET-UP AND DATABASE

4.1 Wind tunnel description

The test was conducted in the A9 wind tunnel in IDR/UPM which is an open circuit suction type Eiffel tunnel with a closed test chamber. The convergent section of the wind tunnel is bi-dimensional with a length of 5.25m and an input section of 4.8m wide and 1.8m high. The test chamber has the following dimensions: Length: 3m × Width: 1.5 × Height: 1.8m. The wind tunnel is driven by nine eight-bladed variable speed fans with nominal power of 10kW capable of producing winds of 5-35m/s. The mounting of the model is made using a turntable installed in the sidewall of the test section of the wind tunnel. See figure 3.

4.2 Instrumentation and sampling rate

A total of 475 pressure tabs were installed on the model of the island and an additional 12 pressure tabs were installed as a reference in a straight line on the ramp forward of the Bolund model. The pressure tabs on the island are distributed at a distance of 0.02m (≈0.4*h*) while the 12 reference tabs were installed 0.04m (≈0.8*h*) apart along a straight line in front of the model. Tabs 15-18 were installed along the 239º line. The distribution of the pressure tabs can be seen in figure 3. Tabs 2-5 were installed with a spacing of 0.01m (0.2*h*) along the 270º line with tab 4 being located on the edge of the Bolund island. Each pressure tabs consists of a brass tube, flushed on the model surface, connected to the data acquisition system by a plastic tube with both having 0.001m inner diameter. The plastic tubes are connected to two 64-ports pressure scanners from Scanivalve Corp. (ZOC33).
Measurements were taken at a rate of 100Hz over 180s for each pressure tab. The measurements for all the pressure tabs were done in 2 block measurements of 256 pressure tabs with the 12 reference pressure tabs always present in each block. A pitot was installed upstream of the model to measure the instantaneous static pressure, $\tilde{p}_\infty$ and the instantaneous total pressure, $\tilde{p}_T$. For each block of 256 pressure tabs, a first set of 128 pressure tabs is measured simultaneously during a first interval of 180s, and a second set of 128 pressure tabs is measured in a second-consecutive interval of 180s. Both the acquisition time of 180s and the sampling frequency of 100Hz are chosen taking into account the limitation of the equipment (maximum buffer size) and technical issues. The acquisition time is selected to assure a good convergence of the statistics. The sampling frequency, which gives rise to associated non-dimensional acquisition frequencies St = fh/U_∞ = 1.02 (5 ms^{-1}), 0.34 (15 ms^{-1}), 0.204. (25 ms^{-1}) was selected anticipating the occurrence of energetic pressure fluctuations for Strouhal numbers, St = 0.01 and St = 0.2 (see point 2) at the detachment. Obviously non-dimensional sampling frequencies St = 0.34 and 0.204 do not fulfil the Shannon theorem for characterising pressure fluctuations with St = 0.2.

4.3 Calculations

The instantaneous pressure coefficient is calculated by $\tilde{c}_p = (\tilde{p} - \tilde{p}_\infty)/\tilde{q}_\infty$ where $\tilde{p}$ is the static pressure measure locally by the pressure tabs and $\tilde{q}_\infty$ is the dynamic pressure at the pitot. Since the installation is normally oriented to determine mean pressure coefficients, C_p, and the scanivalve is a differential scanner, the difference $\tilde{r} = \tilde{p} - \tilde{p}_T$ is recorded, and the instantaneous pressure coefficient is then calculated $\tilde{c}_p = 1 - \tilde{r}/\tilde{r}_\infty$, where $\tilde{r}_\infty = \tilde{p}_\infty - \tilde{p}_T$.
The mean pressure coefficient, C_p, the standard deviation pressure coefficient, $C_{\sigma p}$, and the skewness of the pressure, S_p are calculated respectively

$$C_p = \frac{1}{N}\sum_{n=1}^{N} \tilde{c}_{p,n} \,. \tag{0.1}$$

$$C_{\sigma p} = Q_\infty^{-1}\left(\frac{1}{N}\sum_{n=1}^{N} p_n^2\right)^{\frac{1}{2}} \approx Q_\infty^{-1}\left(\frac{1}{N}\sum_{n=1}^{N} r_n^2\right)^{\frac{1}{2}} . \tag{0.2}$$

$$S_p = \left(\frac{1}{N}\sum_{n=1}^{N} p_n^3\right)\left(\frac{1}{N}\sum_{n=1}^{N} p_n^2\right)^{-\frac{3}{2}} \approx \left(\frac{1}{N}\sum_{n=1}^{N} r_n^3\right)\left(\frac{1}{N}\sum_{n=1}^{N} r_n^2\right)^{-\frac{3}{2}} . \tag{0.3}$$

For the previous calculation of second and third moments of the pressure fluctuation, p, from the readings, r, it is considered that typically the fluctuation of the total pressure at the pitot is typically lesser than the fluctuation of the static pressure on the model, mainly at the detachment.
The Bolund model was manufactured with a scale of 1:230 giving a maximum height for the model of 0.0512m. 3D data for the Bolund Island was obtained from the data provided by Bechmann et al. [2009]. The scaled model was manufactured using Necuron400 material in an automated 3D milling machine with a resolution of 10^{-4}m.

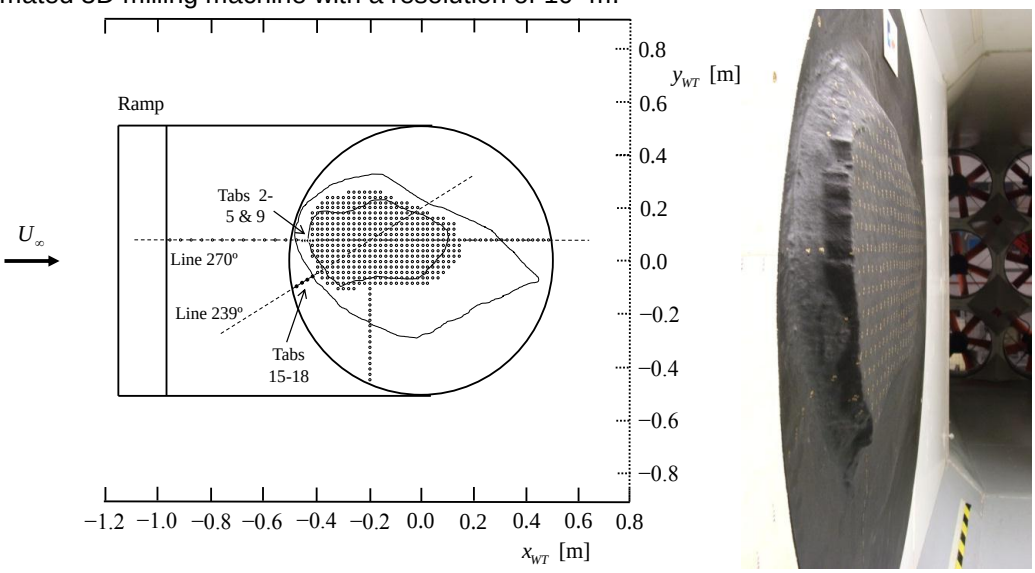

Figure 3: Pressure tabs distribution on the island model and schematic of the mounting in the A9 wind tunnel.

4.5 Measurement Campaign

A total of four angles of wind direction were chosen for the inflow direction. Three angles, 270º, 239º and 255º correspond to the test cases specified in Bechmann et al. [2009]. While the final angle 180º was to be an extra case. The three wind velocities are 5m/s, 15m/s and 25m/s giving a Reynolds number range of $1.7\times10^4 - 8.5\times10^4$ with h=0.0512m. The wind tunnel has a boundary layer thickness, $\delta\approx$ 0.04m and longitudinal turbulence intensity at the reference position $I_u\approx$2.5%.

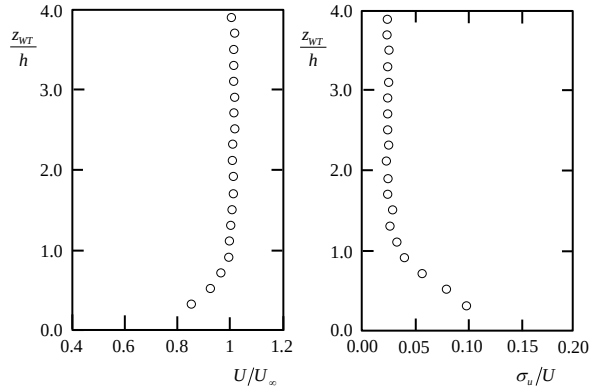

Figure 4: Vertical profiles of mean wind speed and turbulence intensity at at x_{WT}/h=0, at y_{WT}/h=0. Conditions measured without the mock-up.

5 RESULTS

The evolutions for the mean pressure coefficient, C_p, the standard deviation of the pressure coefficient, C_{op}, and the skewness of the pressure, S_p, along the line B (270º) are presented in

figure 5. Results for two Reynolds numbers, Re_h=5.1×10^4 and Re_h=8.5×10^4 are shown. It can be observed that, as expected, a large overpressure occurs just in front of the escarpment due to the blockage produced. Just on the top of the escarpment (x/h=0) a high suction pressure occurs, indicating the presence of separation. The suction pressure reaches maximum values $-C_p \approx 2$ for the higher Reynolds case and $-C_p \approx 1.75$ for the lower Reynolds one. Except for the variation on the maximum value of $-C_p$ the Reynolds number seem not to affect the distribution of mean pressure coefficient, what is in agreement with the conclusions presented in Nakamura & Ozono [1987] for a BFP for $Re_{(2h)} > 1.4\times10^4$. The values of $-C_p$ at the edge are larger than the ones found for right-angled corners-BFP for similar values of $Re_{(2h)}$ [see for instance Li & Melbourne, 1999, where maximum values $-C_p \approx 1.1$ are declared], probably due to the specific geometry of the Bolund escarpment at 270º (with an initial ramp and with a slightly rounded edge).

The evolution of the standard deviation of the pressure coefficient, C_{op}, grows dramatically at the top of the escarpment, reaching a maximum for both Re_h cases slightly downstream of the edge, at $x/h \approx 0.8$. This is an evidence of the presence of detachment. It has been established that location of max(C_{op}) roughly coincides with the mean position of the reattachment, therefore in this case it can be established that $l_R/h \approx 0.8 \pm 0.1$. For similar Reynolds number and δ/h, but lower I_u, Largeau & Moriniere [2007] determined values $l_R/h \approx 3$. Skewness of the pressure shows large positive values up-stream of the escarpment [what is in agreement with the coclusions for FFS shown by Camussi et al., 2008 and Steinwolf & Rizzi, 2006]. After the edge, there is a region $0.1<x/h<1.1$ with $S_p<0$, recovering positive values roughly at $x/h \approx 1.1 \pm 0.1$. This change of sign of S_p (from negative to positive values) has been propossed above as an indication of the reattachment region, so the location of such reatachment based on maxC_{op}, and the sign change of S_p roughly coincide around $x/h \approx 1$.

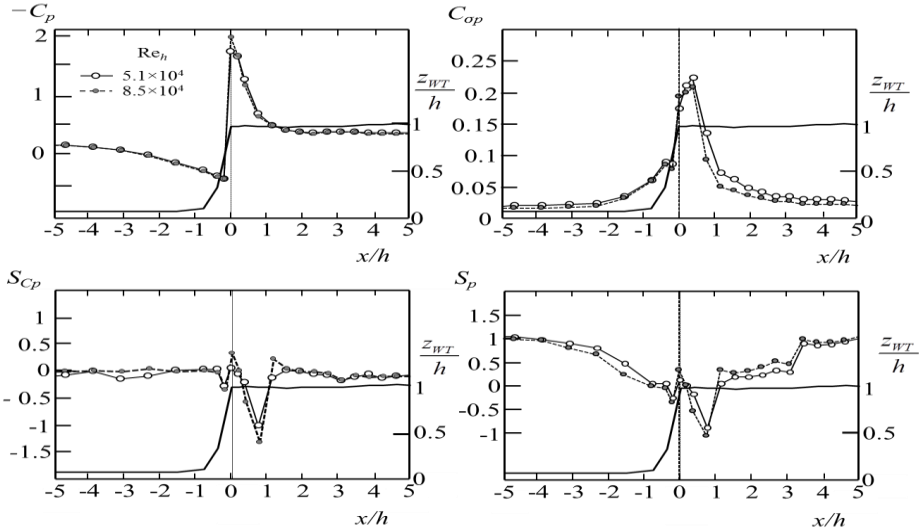

Figure 5: Distribution of mean pressure coefficient, C_p, expression (0.1), standard deviation pressure coefficient, C_{op}, expression (0.2), Skewness of pressure coefficient, S_{Cp}, and skewness of the pressure, S_p, expression (0.3) along line B (270º), for two Reynolds numbers, Re_h, indicated in the figure. The profile of the island for the mentioned direction is shown in the figure in continuous line.

In figure 6 the surface distributions of C_p, C_{op}, and S_p (left-right columns) for line 270º and the two Reynolds numbers (top,bottom). The white color for the two figures in the first column, indicate values $-C_p \geq 1$, therefore the mean topology of the detached bubble. It is evidenced the 3D-like character of such topology and the existence of local patterns that can be easily identified with the geometry of the escarment. For intance the detached region seems to be more intense at the center of the escarpment where the vertical portion of it is larger and faces perpendicular to the 270º wind. The results shown in figures at the second column (C_{op}) corroborates the 3D character of the separated region. The analysis of S_p (third column) reveals a similar conclusion. The white dotted line in the figure marks the loci on the surface where S_p = 0. It must be remarked that S_p values are trustable only when C_{op} is high (as it was argumented

above) so the values of S_p for x/h>3 must not be used to extract any conclusion without a further analysis.

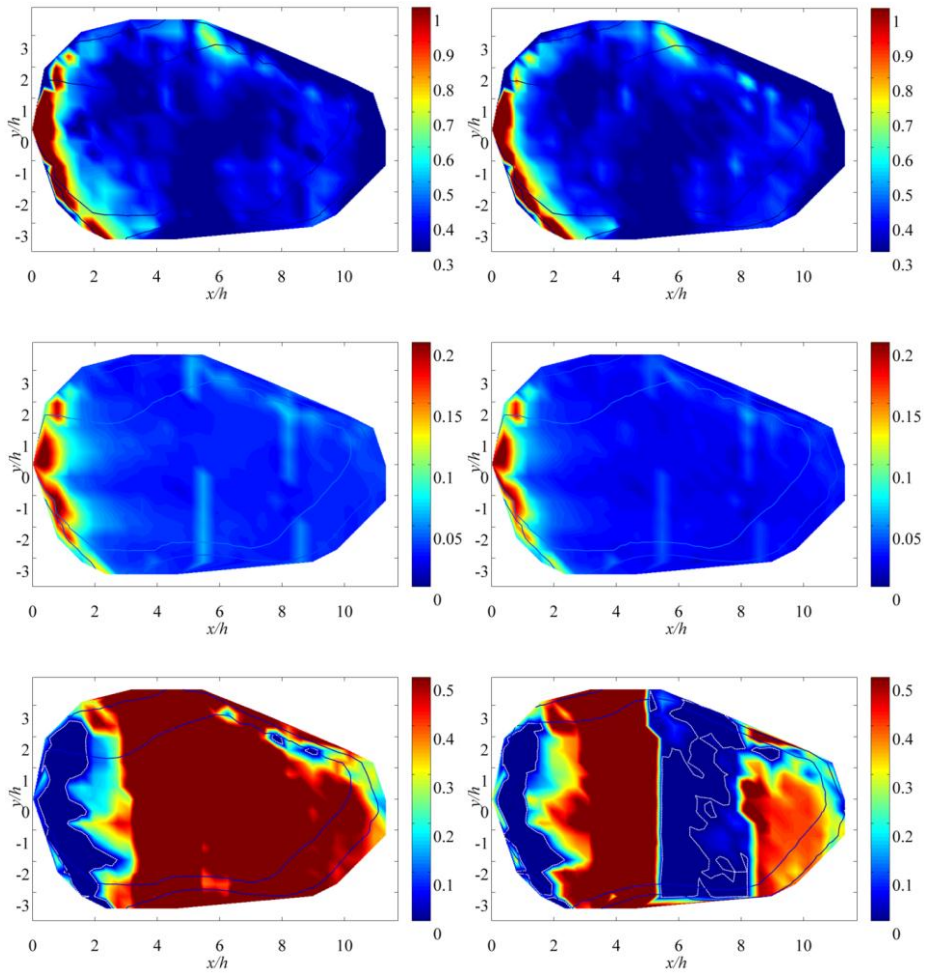

Figure 6: Surface distribution of mean pressure coefficient, C_p, (first column), standard deviation pressure coefficient, C_{op} (second column), and skewness of the pressure, S_p, (third column) along line B (270º), for two Reynolds numbers (top row, Re_h = 5.1×10^4, bottom row, 8.5×10^4). The dark lines indicate isolevel curves, and the white lines indicates the loci where S_p = 0 on the surface.

The same analysis is showed in figure 7 for the 239º case. It is obvious that the region of detachment now appears at regions perpendicular to the 239º wind. It is remarked the appearance of a region of high values of $-C_p$ and C_{op} at the uppper region of the topography probably incating a backward-facing step-like detached region.

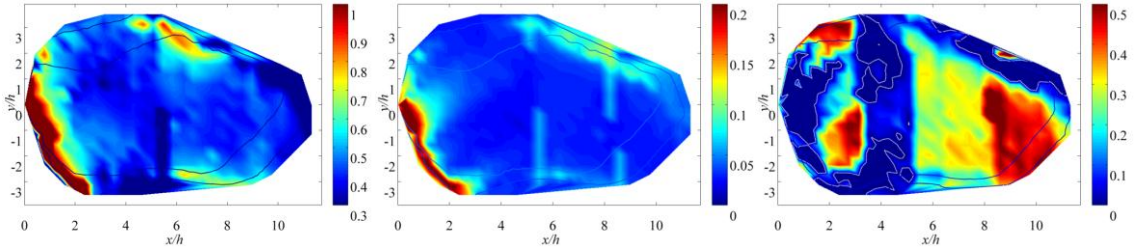

Figure 7: Surface distribution of mean pressure coefficient, C_p, (left), standard deviation pressure coefficient, C_{op} (middle), and skewness of the pressure, S_p, (right) along line A (239º), for a Reynolds number Re_h = 5.1×10^4. The dark lines indicate isolevel curves, and the white lines indicates the loci where S_p = 0 on the surface

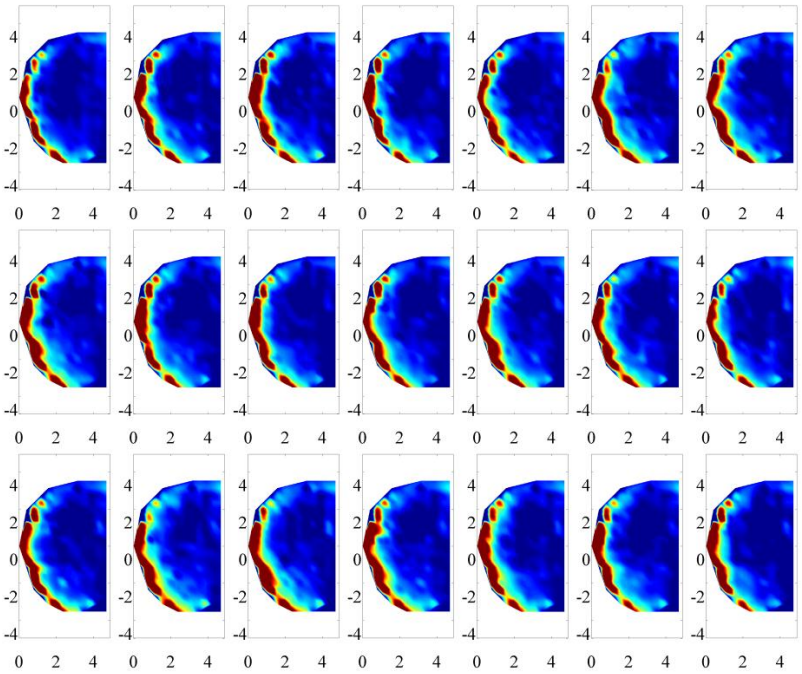

Figure 8: Surface distribution of the instantaneous pressure coefficient, $-\tilde{c}_p$, for the case 270º and at Reynolds number Re_h=8.5×10^4. The color bar is the same as for the C_p figures in figure 6 and 7.

In order to illustrate the non-steadyness of the separation proccess, in figure 8, a sequence of 21 shots of the instantaneous preassure coefficient, $-\tilde{c}_p$, are shown for the case 270º and Re_h = 8.5×10^4. The time interval between shots is Δt=0.01s corresponding to a nondimensional time interval ΔT=4.8 ($T = tU_\infty/h$). It is reminded that flapping process for a FFS takes part (in a mean sense) every $\Delta T_F \approx 100$. It can be realised that the region where is instantaneously $-\tilde{c}_p$>1 changes its shape remarkably.

6 CONCLUSIONS

Surface pressure measurements in the wind tunnel can provide a quick and informative preliminary insight of the detachment region extension of the escarpment. In this case, for the flow over the Bolund Island, studying the statistics of the averages of the pressure distribution, an estimation of the horizontal extension of the detachement bubble size can be obtained.

7 REFERENCES

1. Bechmann, A., Berg, J., Courtney, M.S., Joergensen, H.E., Mann, J., Soerensen, N.N. 2009. The Bolund Experiment: Overview and Background Risoe-R-1658(EN).
2. Bradshaw, P., Wong, F. 1972. The reattachment and relaxation of a turbulent shear layer. Journal of Fluid Mechanics 52; 113.
3. Camussi, R., Felli, M., Pereira, F., Aloisio, G., Di Marco, A. 2008. Statistical properties of wall pressure fluctuations over a forward-facing step. Physics of Fluids 20.
4. Castro, I., Dianat, M. 1983. Surface flow patterns on rectangular bodies in thick boundary-layers. Journal of Wind Engineering and Industrial Aerodynamics 11; 107-119.
5. Conan, B., Buckinham, S., van Beeck, J., Aubrun, S., Sanz-Rodrigo, J. 2011. Feasibility of Micro Siting in Mountainous Terrain by Wind Tunnel Physical Modelling. European Wind Energy Conference Scientific Proceedings; 136-140.
6. Hillier, R., Cherry, N. 1981. The effects of stream turbulence on separation-bubbles. Journal of Wind Engineering and Industrial Aerodynamics 8; 49-58.

7. Huiyin, R., Yanhua, W. 2011. Turbulent boundary layer over smooth and rough forward-facing steps; Physics of Fluids 23.
8. Kiya, M., Sasaki, K. 1983a. Free-stream turbulence effects on a separation bubble. Journal of Wind Engineering and Industrial Aerodynamics 14; 375-386.
9. Kiya, M., Sasaki, K. 1983b. Structure of a turbulent separation bubble. Journal of Fluid Mechanics 137; 83-113.
10. Largeau, J.F., Moriniere, V. 2007. Wall pressure fluctuations and topology in separated flows over a forward-facing step. Experiments in Fluids 42; 21-40.
11. Li, Q., Melbourne, W. 1995. An Experimental investigation of the Effects of Free-Stream Turbulence on Streamwise Surface Pressures in Separated and Reattaching Flow. Journal of Wind Engineering and Industrial Aerodynamics 54; 313-323.
12. Li, Q., Melbourne, W. 1999. The effect of large-scale turbulence on pressure fluctuations in separated and reattaching flows. Journal of Wind Engineering and Industrial Aerodynamics 83; 159-169.
13. Meroney, R.N. 1993. Wind Tunnel Modelling of Hill and Vegetation Influence on Wind Power Availability. Task 1: Literature Review.
14. Nakamura, Y., Ozono, S. 1987. The effects of turbulence on a separated and reattaching flow. Journal of Fluid Mechanics 178; 477-490.
15. Saathoff, P., Melbourne, W. 1989. The generation of peak pressures in separated reattaching flows. Journal of Wind Engineering and Industrial Aerodynamics 32; 121-134.
16. Sherry, M., Lo Jacono, D., Sheridan, J. 2010. An experimental investigation of the recirculation zone formed downstream of a forward facing step. Journal of Wind Engineering and Industrial Aerodynamics 98; 888-894.
17. Steinwolf, A., Rizzi, S. 2006. Non-Gaussian analysis of turbulent boundary layer fluctuating pressure on aircraft skin panels. Journal of Aircraft 43; 1662-1675.
18. Stuer, H., Gyr, A., Kinzelbach, W. 1999. Laminar separation on a forward facing step. European journal of mechanics.B, Fluids 18; 675-692.
19. Tachie, M., Balachandar, R., Bergstrom, D. 2001. Open channel boundary layer relaxation behind a forward facing step at low Reynolds numbers. Journal of fluids engineering 123; 539-544.